

# Diffraction effects in honeycomb arrays of multiwalled carbon nanotubes

Brian Kimball<sup>a</sup>, Joel B. Carlson<sup>a</sup>, Diane Steeves<sup>a</sup>, Krzysztof Kempa<sup>b</sup>, Zhifeng Ren<sup>b</sup>, Pengfei Wu<sup>c</sup>, Thomas Kempa<sup>b</sup>, Glynda Benham<sup>d</sup>, Y. Wang<sup>b</sup>, Wenzhi Li<sup>b</sup>, A. Herczynski<sup>e</sup>, Jacob Rybczynski<sup>c</sup> and D.V.G.L.N. Rao<sup>c</sup>

<sup>a</sup>U.S. Army, Natick Soldier Center, Natick, MA 01760

<sup>b</sup>Boston College, Physics Department, Chestnut Hill, MA 02467

<sup>c</sup>University of Massachusetts Boston, Physics Department, Boston, MA 02125

<sup>d</sup>MegaWave Corporation, Boylston MA 01505

<sup>e</sup>Florida International University, Miami, Florida 33199

## ABSTRACT

Carbon nanotubes were grown on silicon and quartz substrates in a honeycomb configuration using self-assembly nanosphere lithography and plasma enhanced chemical vapor deposition methods. Photonic nanoarrays were fabricated with varying spacing and carbon nanotube height. Both periodic and nonperiodic arrays were produced and evaluated. Optical properties of the arrays were studied and related to array geometry. Three dimensional diffraction maps were created that reveal the manner in which the nanoarrays interact with visible light. The unique optical properties of the arrays combined with the excellent mechanical and electrical properties of carbon nanotubes indicates that these materials may find many uses in the field of optoelectronics.

**Key Words:** Carbon nanotubes, periodic arrays, diffraction efficiency, polarization effects, self-assembly nanosphere lithography.

## 1. INTRODUCTION

Periodic arrays of aligned carbon nanotubes (CNT) have been produced using nanosphere self-assembly<sup>1,2</sup>. These arrays have been studied for a number of applications including field emitters<sup>3</sup> and nanoelectrodes<sup>4</sup>, components for a micro communications system as well as 2-D photonics crystals. Optical studies have been performed detailing the diffraction and polarization properties of periodic CNT arrays<sup>5</sup>. In a previous paper we discussed the general optical properties of CNT arrays based on preliminary experimental observations<sup>1</sup>. The paper also described the concept of using periodic CNT arrays as 2-D photonic crystals in the visible spectrum. Previous studies have described the nonlinear transmission and scattering in solutions of multiwalled CNTs<sup>6</sup>.

In this paper we present some experimental results further documenting the optical properties of aligned, periodic and non-periodic CNT arrays. Diffraction and polarization studies were performed with both monochromatic and white light sources. The results indicated strong polarization dependence for both periodic and non-periodic arrays. Polarized diffracted light is described in terms of efficiency. A peak in diffracted light intensity in the direction of the source has been observed<sup>7</sup> by others and is reported here. We also report a polarization-dependent resonant effect due to the intra-action of visible light with nonperiodic arrays that appears as bright colors to the observer.



Periodic CNT arrays such as these have the potential for numerous applications. The nanotube arrays have unit sizes on the order of a wavelength of visible light and exhibit a strong electromagnetic response. This has allowed for the realization of concepts and devices normally associated with microwaves and radio waves.

## 2. EXPERIMENTAL EVALUATION

Periodic honeycomb arrays and nonperiodic arrays were evaluated for the way in which they interact with electromagnetic radiation in the visible spectrum. A tungsten lamp was used as a white light source. Continuous wave lasers at 442nm, 532nm and 633nm were used as monochromatic light sources. An Ocean Optics Fiber Optic Spectrometer was used to evaluate scattering from the CNT samples. SEM was used to determine sample geometry.

### 2.1 Sample fabrication

Periodic arrays of aligned carbon nanotubes were created using nanosphere self-assembly. The technique employs nanospheres of various sizes ranging from 0.2 to 2  $\mu\text{m}$ . Polystyrene nanospheres are self-assembled on a substrate and used as a mask to create a vapor deposited honeycomb pattern of metallic dots. The dots then serve as the catalyst to grow a periodic array of carbon nanotubes using the plasma enhanced chemical vapor deposition (PECVD) method. Varying the thickness of the catalyst and the dot size can control the diameter of the nanotubes. The dot size is determined by the size of the nanospheres and can be further controlled by plasma etching. The length of the tubes is determined by the growth time, which is generally on the order of about 10 minutes. Recent improvements in the fabrication process have made it possible to create high quality structures<sup>8</sup>. By optimizing parameters such as heating temperature, deposition thickness of catalytic dots, plasma current intensity and pre-growth plasma etching time it is possible to improve long range periodicity and uniformity of CNT diameters, straightness and length. Thus it is possible to create nanostructures with varying feature size and spacing that will interact strongly with electromagnetic radiation for wavelengths on the order of the unit size. Figure 1 shows a CNT array created using 1.5  $\mu\text{m}$  nanospheres.

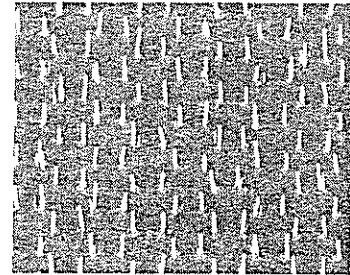


Fig. 1. Multiwalled carbon nanotubes honeycomb array fabricated using self-assembly nanosphere lithography. Sample was created with 1  $\mu\text{m}$  polystyrene nanospheres.

### 2.2 Diffraction studies

Diffraction studies indicate that the response of the periodic arrays conforms to Bragg's law:

$$n\lambda = d \sin \theta, \quad \text{Eq. 1}$$

where  $\lambda$  is the wavelength,  $\theta$  is the angle of diffraction and  $d$  is the distance between point scatterers. Characteristic spacing ( $d$ ) in a honeycomb array can be described in terms of the diameter of the nanosphere used to create the catalyst pattern. Along one direction the spacing is equal to the diameter of the nanosphere. When the sample is rotated 30° in plane, a spacing of  $d=r\sqrt{3}$ , where  $r$  is the nanosphere radius, projects a diffraction pattern that again conforms to Eq 1. Due to symmetry, a wavelength at a given angle will repeat with every 60° of sample rotation. In general, light is diffracted by the honeycomb lattice into Fourier components forming a reciprocal lattice in the form of a two-dimensional triangular pattern (Figure 2). A three-dimensional lattice can be envisioned by forming a series of parallel lines (G-lines) through each point of the reciprocal lattice at locations described by Equation 2<sup>1</sup>.

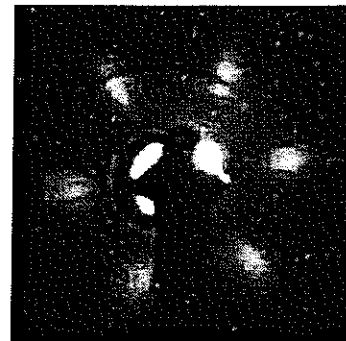


Fig. 2. Diffraction pattern generated by honeycomb periodic CNT array.

$$\mathbf{G} = mb_1 + nb_2. \quad \text{Eq. 2}$$

The Ewald sphere governs the order of diffraction. The sphere is superimposed over the G-lines and reciprocal lattice, and has a radius equal to the wave vector  $k$ , given by

$$|k| = \frac{2\pi}{\lambda}. \quad \text{Eq. 3}$$

For this lattice

$$|G| = s \sqrt{\frac{3m^2}{4} + \left(\frac{m}{2} + n\right)^2}. \quad \text{Eq. 4}$$

Three-dimensional diffraction maps were created by measuring the radar cross-section reflected from the sample at in-plane angles relating to a Bragg diffracted beam. The radar cross-section is the signal that is reflected directly back to the illuminating probe. Radar cross-section measurements were obtained via a fiber optic back-reflection probe. By recording spectra at varying angles of incidence, and assembling them in a single graphic we created diffracton maps. Figure 3 shows a series of three dimensional diffraction maps. These data were acquired from three different samples with identical spacing, but with varying CNT length. Immediately apparent in the plots is that the Bragg wavelength signature is identical for each. This component of the response relates to the inter-effects of the combined scatterers. Note however, that the signal peak occurs at a different wavelength for each sample. This suggests that the observed wavelength is a function of the length of the individual scatters. This component is due to the intra-effects of the individual scatterers. We wish to demonstrate that resonance occurs due to the interaction of CNTs of specific length when illuminated with light of a specific wavelength, and angle of incidence. This interaction can be described in a way that is similar to the way in which radio waves interact with antennas. For a random array of dipole antennas mounted normally on a dielectric substrate, the condition for maximum response is given by

$$L = m \frac{\lambda}{2} f(\theta, n) \quad \text{Eq. 5}$$

where  $L$  is the dipole length,  $\lambda$  is the resonant wavelength and  $\theta$  is the angle of incidence<sup>8</sup>. For a single dipole antenna (Figure 4),  $f(\theta, n) = 1$ , and the expression reduces to the familiar dipole antenna response. If the distance  $D$  between dipoles is  $D \ll \lambda$ , then  $f(\theta, n) = (n^2 - \sin^2 \theta)^{-1/2}$ . For  $D \gg \lambda$  or  $D \sim \lambda$ ,  $f(\theta, n) \approx 1$ , and the response is only weakly dependent on  $\theta$ . The polarization is such that the electric field component aligned with the longitudinal axis of the dipole. By modeling CNTs as a random array of dipole antennas<sup>9</sup>, and studying the resonant behavior of nonperiodic CNT samples we were able to observe the response of

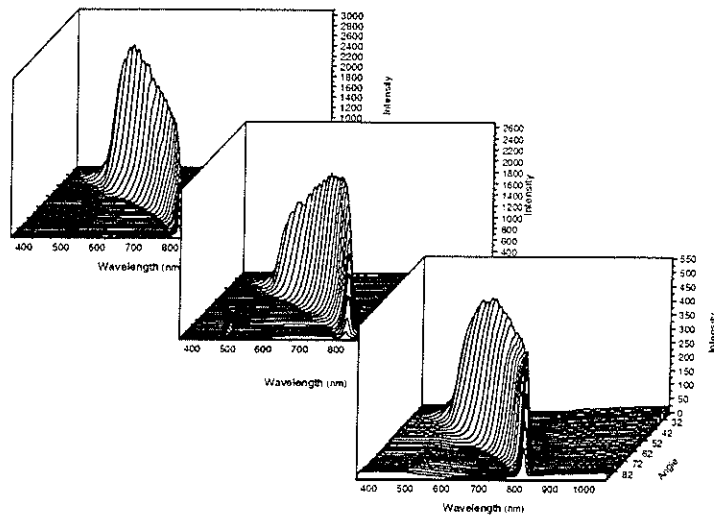


Fig. 3. Wavelength vs. intensity vs. incident angle for three CNT samples with identical CNT spacing, but with varying CNT height

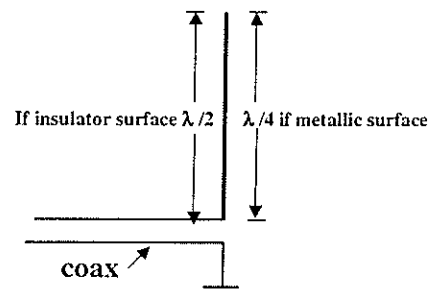


Fig. 4. Carbon nanotube modeled as quarter-wave, vertical dipole, ground-plane antenna. Radiation pattern is doughnut shaped about the longitudinal axis.

individual scatterers separate from the diffraction effects of periodic scatterers. Nonperiodic CNT samples were created with gradually varying CNT height (Figure 5a). This was accomplished by creating an uneven electric field over the sample surface during CNT growth. Spectroscopic measurements were taken at various locations on the samples (Figure 5b). SEM was used to determine the heights of the nanotubes at the respective locations. Figure 6 shows a micrograph of the nonperiodic sample that exhibits colors. Also shown is an SEM image of dislodged CNTs from which length measurements were obtained. A computer model was used to generate a series of curves that relate to a resonant condition with respect to random dipole antenna length. These curves are shown in Figure 7. Experimental data for various nonperiodic CNT arrays are also shown. The experimental results show good agreement with the predicted dipole response. Results indicate that the colors observed, both spectroscopically and visibly in the nonperiodic samples, are the result of a resonant interaction between incident white light and the individual nanotubes. The nanotubes interact with visible light in much the same way as radio waves interact with radio antennas.

### 2.3 Nonperiodic CNT array polarization response

The polarized response of aligned, nonperiodic CNT arrays is primarily with the electric field component parallel to the longitudinal axis of the nanotubes (*p*-polarized). This is shown in Figure 8. The silicon sample has two zones, one with a random array of aligned CNTs and the other with a thin metallic Cr film. It can be seen that the CNT array efficiently scatters *p*-polarized light for the case of

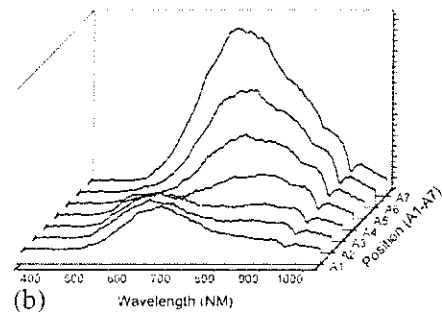
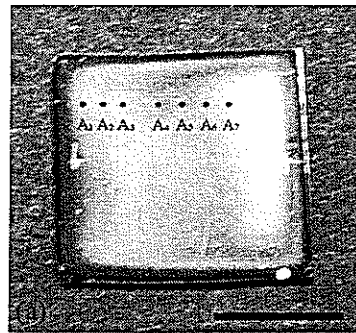


Fig. 5. Antenna length matching effect<sup>8</sup>. (a) Interference colors from the random array of aligned MWCNTs. A<sub>1</sub> – A<sub>7</sub> are the selected positions where the length and optical measurements were carried out. Scale bar, 1 cm. (b) Experimental reflected wavelength response measured at selected points on the sample shown in (a).

polarization angle,  $\Theta = 0^\circ$ . Whereas the darkness of the metal film indicates a lack of interaction with light polarized in this way. For the case of *s*-polarized light, the trend is reversed with the CNT zone showing inefficient scattering of light while the metal zone shows strong reflectance.

The strong interaction of aligned CNT arrays with *p*-polarized light is due to movement of electrons along the longitudinal surface of the individual CNTs. For the thin metal film, the free electron motion is in plane, thus there is a greater response to *s*-polarized light. A series of images were acquired similar to those shown in Figure 8. Individual datums relate to orientations of the observed linear polarization ( $\Theta$ ). Relative irradiances were recorded for both the metal and CNT zones of the sample and

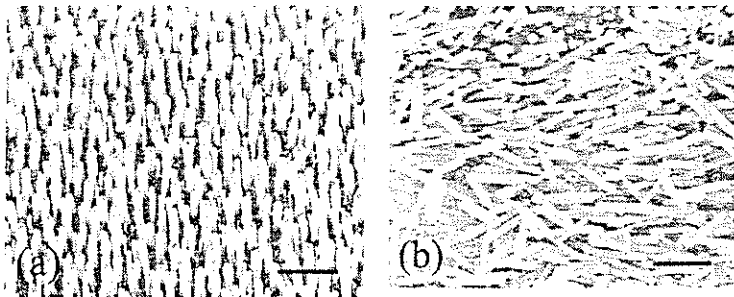


Fig. 6. Aligned (a) and scratched (b) random arrays of MWCNTs<sup>8</sup>. Scale bars, 1  $\mu\text{m}$ .

plotted versus the angle  $\Theta$ . These data are plotted in Figure 9 with a theoretical curve given by the law of Malus, which describes the irradiance of polarized light passing through an analyzer with rotating transmission axis. In this case the high, linearly polarized response of the multiwalled CNTs acts as the analyzer.

$$I(\Theta) = \frac{c\epsilon_0}{2} E_0^2 \cos^2 \Theta \quad \text{Eq. 6}$$

The maximum irradiance is given by

$$I(\Theta) = \frac{c\epsilon_0}{2} E_0^2 \quad \text{Eq. 7}$$

and occurs when  $\Theta=0$ . The response of the thin metallic film is 90 out of phase with the CNT response and thus can be described by

$$I(\Theta) = \frac{c\epsilon_0}{2} E_0^2 \sin^2 \Theta \quad \text{Eq. 8}$$

### 2.4 Periodic CNT array polarization response

For periodic samples illuminated with monochromatic light, the polarization response was found to differ significantly from that of the non-periodic array. To study the polarization response of periodic samples we evaluated the diffraction efficiency of three wavelengths in the visible region at varying incident angles for incident *s*- and *p*-polarization. CNT, honeycomb arrays were evaluated with cw lasers at 442nm, 532nm and 633nm.

When the periodic CNT sample is irradiated normal to the surface, a diffraction pattern is formed as shown in Figure 2. The sample was positioned such that two of the diffraction spots from the monochromatic light sources were located on either side of the incident plane. The intensity of each of the two diffracted beams was measured as a function of angle of incidence for both *s*- and *p*-polarization using a photodetector. It is evident in Figure 10 that each wavelength has an angle of incidence for which the irradiance of the diffracted beam is a maximum. For 633nm the angle is 20°, for 532nm it is 17° and for 442nm the angle is 14°. At these angles the incident and scattered beam are exactly superposed. This characteristic has been previously observed in random scattering media. The enhanced backscattering it attributed to constructive interference occurring between the incident beam and a beam scattered directly back to the source from the scattering medium. In the honeycomb array, the electromagnetic field is localized about the nanotubes scatterers. The resonant states can propagate from one scattering site to another. If the wave vectors travel in opposite directions with the same phase, then constructive interference

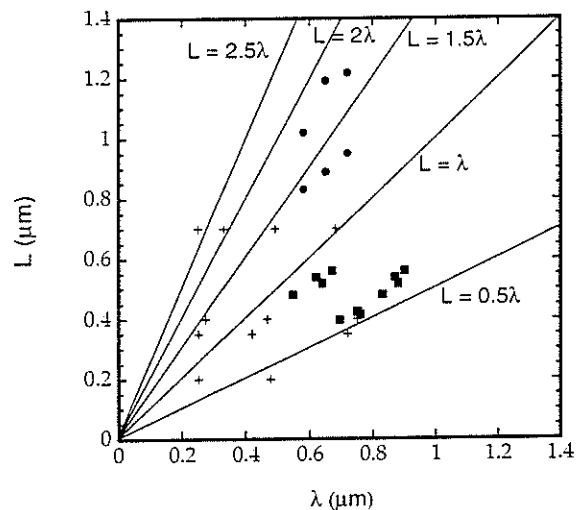


Fig. 7. Antenna length matching effect<sup>8</sup>. Average length (*L*) of MWCNTs vs. wavelength ( $\lambda$ ) of the incoming radiation at the corresponding maxima of reflected intensity. From sample evaluated using a fiber optic sensor (squares), and a CCD camera (circles). Solid lines represent the simple dipole antenna condition (Eq. 1). Crosses mark maxima of the reflected intensity spectra, shown in Fig. 5.

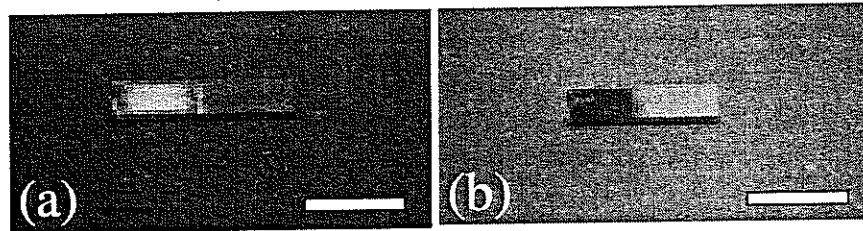


Fig. 8. Polarization effect. A random array of aligned nanotubes (left side of the sample) next to a thin metallic (Cr) film (right side of the sample) observed through a polarizer at two orientation angles  $\Theta$ . (a) Polarization plane parallel to nanotubes (*p*-polarization)  $\Theta = 0^\circ$ . (b) Polarization plane perpendicular to nanotubes (*s*-polarization),  $\Theta = 90^\circ$  Scale bars, 1  $\mu\text{m}$ .

can occur between the backward and forward propagating waves.

The polarization response indicates that *s*-polarized light is scattered more efficiently than *p*-polarized light. This is not consistent with the dipole model where antenna-like resonance occurs when the *e*-field is aligned with the longitudinal axis of the nanotubes. This response has been attributed to the geometry of the multiwalled CNT, which are essentially concentric cylinders of rolled graphite sheets<sup>10</sup>. Electrons can move more easily within a single cylinder than from one concentric cylinder to another. Electrons that are excited by *s*-polarized light move freely within a single sheet. Whereas *p*-polarized light, except for the case of 90° incidence, has a component that requires movements across sheets and hence is inherently less efficient.

Also evident in Figure 10 is that the shortest wavelength is scattered most efficiently. This is expected from general electromagnetic scattering theory.

### 3. SUMMARY

The optical properties of honeycomb, periodic arrays of CNTs have been documented. Polarization measurements indicate that the intensity of both the diffracted light and diffusely scattered light is dependent on wavelength and angle of incidence. It is believed that these observations are related to scattering efficiency due to combinations of a number of effects such as nanotube length, width, spacing, angle of incidence and polarization of incident light. Future studies will deal with varying nanotube array geometry, and evaluating and comparing results.

Experimental results indicate that for a periodic array, there was a strong *s*-polarization response, whereas for a nonperiodic sample the response was greater for *p*-polarization. The discrepancy may have been due to resonance occurring in different regions of the spectrum not common to both samples. It is known that the optical response for CNT arrays is greatly dependent upon array geometry. The CNTs in the nonperiodic sample were longer (several microns) than those in the periodic samples (500nm).

If antenna-like resonance is present, it is reasonable to expect that the resonance can be enhanced in terms of gain and directionality. By arranging CNTs in periodic arrays fashioned after radio or microwave antenna arrays, it should be possible to realize high gain and directionality for specific wavelength bands. Numerous antenna designs exist and have been utilized for many years in radar, television, and FM, short wave and AM radio that can serve as models for this purpose (Figure 11). Devices such as these await microelectronic components that are

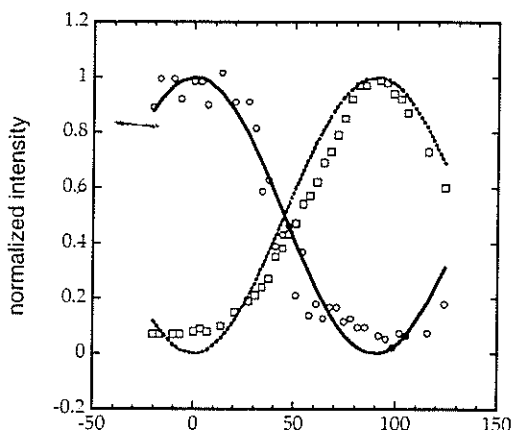


Fig. 9. Polarization effect. Reflected normalized light intensity vs. polarization angle  $\Theta$  for the sample shown in Fig. 2. Circles represent the light intensity from the random array of aligned nanotubes, and squares from the metallic film. Lines represent the expected

functional dependencies:  $I = \cos^2 \theta$  for nanotubes (solid),  $I = \sin^2 \theta$  for metallic film (dashed)<sup>8</sup>.

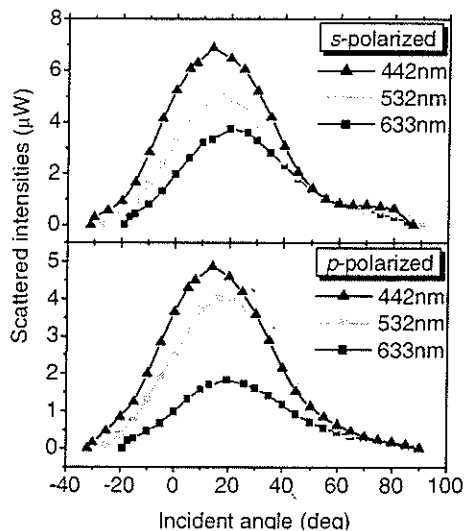


FIG. 10. Dependence of scattered intensities on incident angle with different incident wavelengths and polarizations. Three cw lasers: 633nm He-Ne, 532nm Nd:YAG and 442nm He-Cd were used as incident beams. The incident beam diameter was about 2mm on the sample surface. The intensity was 1 mW for both *s*- and *p*-polarized beams of all wavelengths<sup>10</sup>.

capable of handling these high optical frequencies.

The unique optical properties of these arrays make them excellent candidates for use as optical filters, and communication demodulators and demultiplexers. These arrays may allow for the realization of new optical materials and electro-optical devices that are small, lightweight and require little or no power. In addition to their optical properties, periodic CNT arrays have a host of other unique electromagnetic and mechanical properties that can be exploited for numerous applications. These arrays not only reflect and diffract light, but can also have a photonic band gap in, or around, the visible frequency range. The precise frequency location and size of this gap can be controlled by the structural and material parameters of the arrays.

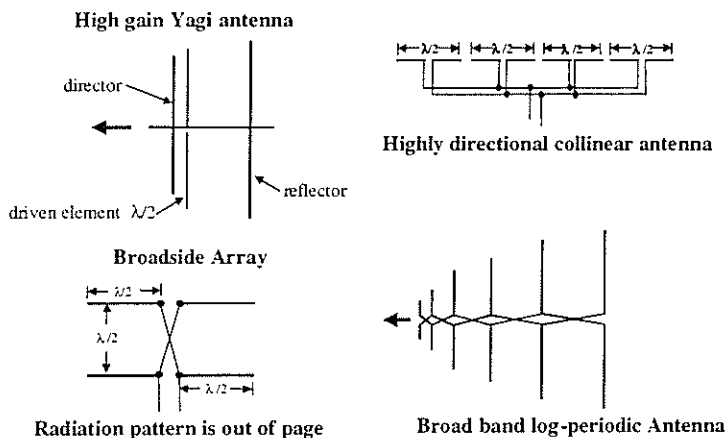


Fig. 11. Various antenna designs can be utilized to control directionality and high gain within a device, thus minimizing power requirements and optical component cross talk.

## REFERENCES

1. K. Kempa, B. Kimball, J. Rybczynski, Z. P. Huang, P.F. Wu, D. Steeves, M. Sennett, M. Giersig, D.V.G.L. Rao, D.L. Carnahan, D.Z. Wang, J.Y. Lao, W.Z. Li and Z. F. Ren, "Photonic Crystals Based on Periodic Arrays of Aligned Carbon Nanotubes", *NanoLetters* **3**, 13–18 (2003).
2. Z. P. Huang, D. L. Carnahan, J. Rybczynski, M. Giersig, M. Sennett, D. Z. Wang, J. G. Wen, K. Kempa, Z. F. Ren, "Growth of Large Periodic Arrays of Carbon Nanotubes", *Appl. Phys. Lett.* **82**, 460–462 (2003).
3. S. H. Jo, Y. Tu, Z. P. Huang, D. L. Carnahan, D. Z. Wang, Z. F. Ren, "Effect of length and spacing of vertically aligned carbon nanotubes on field emission properties", *Appl. Phys. Lett.* **82**, 3520–3522 (2003)
4. Y. Tu, Yuehe Lin, Z.F. Ren, "Nanoelectrode Arrays Based on Low Site Density Aligned Carbon Nanotubes", *NanoLetters*, **3**, 107–109 (2003).
5. B. Kimball, J. Carlson, K. Kempa, W. Li, Z. Ren, P. Wu, D.V.G.L.N. Rao, J. Rybczynski, M. Giersig, Z. Huang, D. Carnahan, D. Steeves, M. Sennett, SPIE Proc. Vol. 5224, August 2003.
6. Steeves, D., Kimball, B. R., "Nonlinear Transmission and Scattering of Multiwalled Carbon Nanotubes Suspended in an Index Matched Solid Matrix and Optical Dye Solution", SPIE Proc. Vol. 4797, July 2002.
7. A. R. McGurn, A. A. Maradudin, and V. Celli, *Phys. Rev. B* **31**, 4866 (1985). Cassagne, D.; Jouanin, C.; Bertho, D. *Phys. Rev. B* **53**, 7134 (1996).
8. Y. Wang, J. Rybczynski, D. Z. Wang, W. Z. Li, B. Kimball, K. Kempa, and Z. F. Ren, Submitted to *Appl. Phys. Lett.*, under review.
9. These calculations use the Numerical Electromagnetics Code, NEC-4 1D, authored by G. Burke et al, Lawrence Livermore National Laboratory
10. Pengfei Wu, B. Kimball, J. Carlson and D. V. G. L. N. Rao, *Phys. Rev. Lett.* (In print)